Flow of foam past an elliptical obstacle

Benjamin Dollet,[1,*] Mélanie Durth,[1] and François Graner[1]
[1]*Laboratoire de Spectrométrie Physique, Boîte Postale 87, 38402 Saint-Martin-d'Hères Cedex, France*
(Received 5 January 2006; published 8 June 2006)

To investigate the link between discrete small-scale and continuous large scale mechanical properties of a foam, we observe its two-dimensional flow in a channel, around an elliptical obstacle. We measure the drag, lift, and torque acting on the ellipse versus the angle between its major axis and the flow direction. The drag increases with the spanwise dimension, in marked contrast with a square obstacle. The lift passes through a smooth extremum at an angle close to, but smaller than 45°. The torque peaks at a significantly smaller angle 26°. No existing model can reproduce the observed viscous, elastic, plastic behavior. We propose a microscopic visco-elasto-plastic model which agrees qualitatively with the data.

DOI: 10.1103/PhysRevE.73.061404 PACS number(s): 83.80.Iz, 47.50.Ef, 47.50.Cd, 82.70.Rr

A foam is a model to study materials which are viscous, elastic, and plastic. This complex, ubiquitous behavior is exploited in numerous applications, such as ore separation, drilling and extraction of oil, food or cosmetic industry [1], but is not yet fully understood [2]. Foam rheology is thus an active research area, and recent studies provide insight to understand the interplay between the bubble scale and the whole foam behavior [3,4] and to unify elasticity, plasticity, and viscosity [5]. Here, we study the flow of foam around an ellipse, where the measured lift, drag, and torque show the whole complexity of foam rheology, which strongly constrains possible models: simple ones do not capture the observed features. We propose an elastoplastic model which describes the data well. We discuss the generality, implications, and limitations of this model.

We have built a foam channel [6] to investigate a two-dimensional (2D) steady flow and measure the force it exerts on an obstacle (Stokes experiment [6–10]). Briefly, a 1 m long, 10 cm wide tank is filled with deionized water with 1% of commercial dish-washing liquid (Taci, Henkel). Its surface tension is $\gamma=26.1\pm0.2$ mN m^{-1}, and its kinematic viscosity is $\nu=1.06\pm0.04$ mm s^{-2}. Several computer controlled injectors blow nitrogen in the solution to form a horizontal monolayer of bubbles of average thickness $h=3.5$ mm, confined between the bulk solution and a glass top plate (quasi-2D foam) [11]. This foam is monodisperse (bubble area at channel entrance: $A_0=16.0\pm0.5$ mm^2) and its fluid fraction is estimated to be around 7% [12].

We study here the simplest shape whose symmetry is low enough to observe simultaneously drag, lift, and torque: the ellipse (Fig. 1). The obstacle has a major axis $2a=48$ mm and minor axis $2b=30$ mm. It floats freely just below the top glass surface, without solid friction. The upper end of an elastic fiber passes through a hole in the bottom of the obstacle, ensuring its free rotation, while its lower end is fixed, so that a top view of the obstacle displacement from its position at rest measures, with a precision better than 0.1 mN, the force exerted by the foam on the obstacle.

We measure the drag in the parallel orientation ($\theta=0$), which is stable (see below); and in the perpendicular one ($\theta=90°$), which is unstable (but where the ellipse can remain for one hour, enough to perform steady flow measurements). The results (Fig. 2) are very close to that for circles of diameters 30 and 48 mm, respectively: this suggests [see also Fig. 4(a)] that drag is proportional to the spanwise direction (along the y axis) l of the ellipse:

$$l = 2\sqrt{a^2 \sin^2\theta + b^2 \cos^2\theta}. \quad (1)$$

In a steady flow (530 ml min^{-1}, i.e., a velocity of 2.5 cm s^{-1}), we start from a given initial orientation (76°, 64°, 48°, or 18°), let the ellipse rotate freely to its parallel stable orientation, and measure the angle, drag, and lift (Fig. 3). The angular velocity strongly increases in the range $15°<\theta<40°$ (with a peak at 26°) and does not depend on the initial orientation (inset of Fig. 3). Moreover, the forces correlate to θ; we thus eliminate the time and plot the dependence of drag and lift with θ [Fig. 4(a)]. All the force data collapse on two master curves, one for the drag and one for the lift. The drag increases roughly linearly with θ except very close to 0° and 90°, where it is extremal by symmetry (it equals 4.5 mN for 0° and 8.8 mN for 90°). As suggested before, the experimental angular dependence of the drag is close to the one of the spanwise dimension, despite small discrepancies for angles close to 0° and 90°. The lift vanishes at 0° and 90°, as expected by symmetry; it is negative (downwards) for angles between 0° and 90°, with a maximal

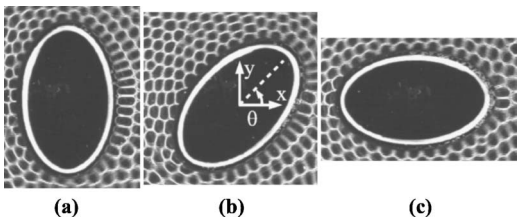

FIG. 1. Top view of the elliptical obstacle and of the surrounding bubbles. Ellipse (a) perpendicular to the flow, (b) tilted in the flow, (c) parallel to the flow. The x axis is the direction of the flow direction and of positive drag, y is the direction of positive lift, and θ (between 0° and 90°, by symmetry) is the angle between x and the major axis of the ellipse.

*Present address: Physics of Fluids, University of Twente, P.O. Box 217, 7500AE Enschede, The Netherlands. Electronic address: b.dollet@utwente.nl

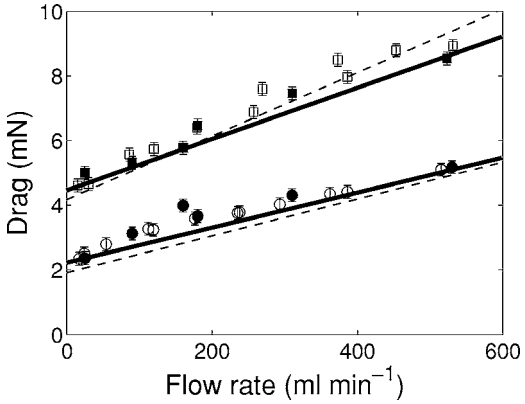

FIG. 2. Drag exerted by the flowing foam on an elliptical obstacle, versus the flow rate. ●: θ=0° [Fig. 1(a)]; ■: θ=90° [Fig. 1(c)]. Bold lines are linear fits to the data. Data (open symbols) and fits (dashed lines) for circular obstacles (○: 30 mm; □: 48 mm diameter) from Ref. [6] are plotted for comparison.

absolute value of 3 mN at an angle of about 40°.

These measurements are independent of the initial orientation, even in the region of quickest variation (inset of Fig. 3). This suggests that the results, obtained in transient regimes, would be the same if we could fix θ to perform steady flow measurements. In fact, at a lower flow rate (25 ml min^{-1}), we observe very similar tendencies, although more noisy (data not shown). It is thus natural to neglect the obstacle's inertia, and assume that the torque exerted by the flowing foam is exactly balanced by a friction torque (arising mainly from viscous dissipation in the capillary bridge between the ellipse and the top plate). Furthermore, the angular velocity $|\dot{\theta}|$ is lower or comparable to 1° s^{-1} [Fig. 4(b)], hence the associated Reynolds number $a^2|\dot{\theta}|/\nu$ does not exceed 10. We can thus assume that the friction torque is proportional to the angular velocity $\dot{\theta}$, then Fig. 4(b) represents (up to an unknown multiplicative constant characterizing the

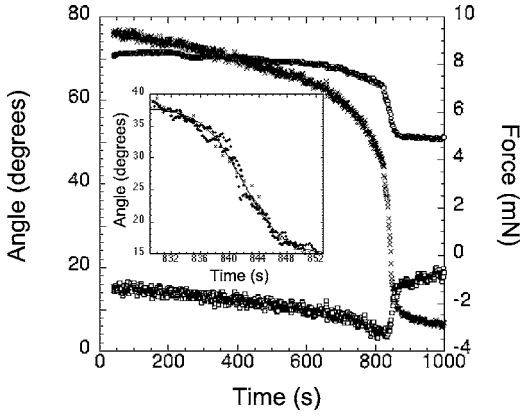

FIG. 3. Angle (×), drag (○), and lift (□) of the ellipse, versus time, for an initial angle of 76°. Inset: zoom on the region of quick variation of the angle. The data for three different initial orientations (×: 76°, +: 64°, △: 48°) are superimposed, by translating the time axis. The solid line is a fit to all data with a hyperbolic tangent profile, indicating that the maximum angular velocity is -2.1 ± 0.1° s^{-1} for an angle of 26.4 ± 0.1°.

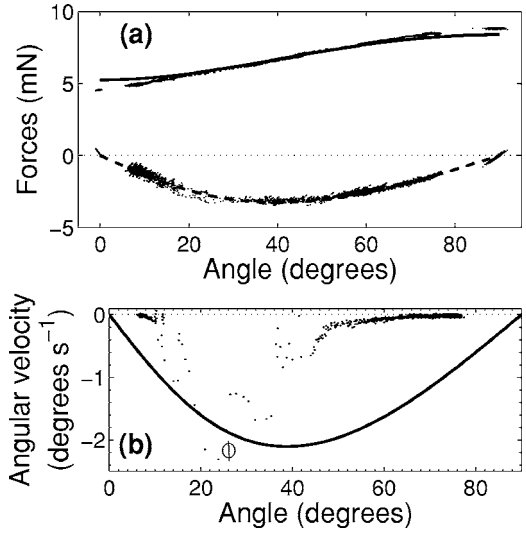

FIG. 4. (a) Drag (positive values) and lift (negative values), (b) angular velocity $\dot{\theta}$ versus θ. Data correspond to the time-dependent experiments with four initial orientations: 76° (same data as in Fig. 3), 64°, 48° and 18°. Also shown for lift and drag are data from the steady orientations, θ=0° and 90°. In (a), the plain curve is the fit by the spanwise dimension (1), and the dashed one is the fit by Eq. (2) for the lift; both fits are up to a free prefactor. In (b), data for $15° < \theta < 40°$ are noisy but compatible with the inset of Fig. 3 (open circle). The curve is the fit by Eq. (2), in arbitrary units.

dissipation) the torque exerted by the foam. It displays a peak around 26°, compatible with Fig. 3.

Figure 4(b) shows that the torque is negative for all positive θ values. Thus the only stable orientation of the ellipse is the parallel one, θ=0°. This contrasts with the Newtonian case, where long objects settle broadside-on [13]. Note that in the case of a Stokes flow (without inertia or elasticity), every orientation of the ellipse would be neutrally stable in an unbounded fluid [14], but that in the presence of boundaries, the parallel orientation is more stable [15]. On the other hand, this is coherent with studies in other non-Newtonian fluids, where ellipses settle broadside-along under gravity in Oldroyd-B fluids [15] or spherical particles aggregate vertically during sedimentation in shear-thinning fluids [16]. Actually, the stable orientation of long objects under flow is determined by a competition between inertia and viscoelasticity [17], which have opposite effects.

Figure 4(a) shows that the lift is oriented downwards, as for a cambered airfoil, probably due to the positivity of the first normal stress difference [18]: this should therefore be valid for every viscoelastic fluid [15]. It is worth noting that lift [Fig. 4(a)] and torque [Fig. 4(b)] are not maximal at the angle of 45°. This contrasts with the existing prediction of the torque exerted on an ellipse by a second-order fluid in potential flow [20], which predicts an angular dependence of the form $\cos\theta \sin\theta$. We suggest two possible explanations for this discrepancy. First, the flow of foam is not potential, and even breaks the $x \to -x$ symmetry between upstream and downstream [21]. Second, second-order fluids might not be good models for foams, because they do not include yield stress.

In yield stress fluids, viscoplastic models predict that the

drag on circular obstacles is proportional to the radius of the obstacle [22] as long as the yield stress remains the preponderant contribution to the total stress. This agrees with experiments on circles [6], and this is compatible with the proportionality of the drag with the leading length of the ellipse (Fig. 2). However, this scaling with the leading length does not hold for a square obstacle, which experiences a drag independent of its orientation [6] for reasons we do not understand yet. In addition, any orientation of a square obstacle is neutrally stable in a flowing foam [6], whereas it would align its diagonals streamwise and spanwise in a viscoelastic liquid, as reported in Ref. [15].

To summarize, we are not aware of a single macroscopic, continuous (viscoelastic or viscoplastic) model which can explain the whole set of experimental data. We now propose an elastic, microscopic model, to catch the main qualitative features of drag, lift, and torque. We estimate the contribution $\vec{F}$ of the soap film tension (which determines the normal tensile elastic stress [1,19]) to the force on the ellipse. Since the foam is quasi-2D, each film separating two bubbles in contact with the obstacle exerts on it a force directed along the film; its magnitude is the line tension λ, which is twice the air-water surface tension γ, multiplied by the foam height h, and a prefactor accounting for 3D geometry [18]. If the flow is quasistatic, the film is along the normal $\vec{n}$ to the surface of the ellipse (see Fig. 1). The total force is thus a sum performed over the films in contact with the ellipse $\vec{F}=\Sigma\lambda\vec{n}$. We do not model the contribution of the bubbles' pressure, which is of the same order of magnitude, and is roughly proportional, to the contribution of the film tension [21,23]. We do not model either the velocity-dependent forces and torque, originating from the viscous friction within the lubrication films between the ellipse and the surrounding bubbles.

If the ellipse is much larger than the bubbles, we consider the distance between consecutive films along the ellipse as a continuous function $f(\alpha)$, α being the angle in the ellipse's parametric equation: $X(\alpha)=a\cos\alpha$, $Y(\alpha)=b\sin\alpha$, and write the force $\vec{F}$ and torque C as integrals:

$$\frac{\vec{F}}{\lambda}=\int\frac{\vec{n}(\alpha)}{f(\alpha)}d\alpha=ab\int_0^{2\pi}\left(\frac{\cos\alpha}{a}\vec{e}_X+\frac{\sin\alpha}{b}\vec{e}_Y\right)\frac{d\alpha}{f(\alpha)},$$

$$\frac{C}{\lambda}=\int\vec{r}(\alpha)\wedge\frac{\vec{n}(\alpha)}{f(\alpha)}d\alpha\cdot\vec{e}_z=(a^2-b^2)\int_0^{2\pi}\frac{\cos\alpha\sin\alpha}{f(\alpha)}d\alpha. \tag{2}$$

We then deduce the drag and lift as $F_x=F_X\cos\theta-F_Y\sin\theta$, and $F_y=F_X\sin\theta+F_Y\cos\theta$, respectively.

We must now model the function f, or equivalently, the deformation of bubbles around the obstacle. As already mentioned in Ref. [18], this is strongly correlated to the local structure of the flow: if it converges towards the obstacle (leading side), it squashes the bubbles in contact, and f is high. Conversely, if the flow diverges from the obstacle (trailing side), it stretches the bubbles in contact, and f is low. Experimental images support this argument (Fig. 1), and, more precisely, lead us to set a phenomenological expression for f. Figure 1 shows that the bubbles remain squashed over the whole leading side [$\beta\leqslant\alpha\leqslant\pi+\beta$ with $\beta=\arctan(b\cot\theta/a)$ from elementary geometry]; we thus assume that f takes a maximum value, f_M over this interval. At the trailing side, Fig. 1 shows that the bubbles are progressively stretched up to a maximum close to the $y=0$ point, or equivalently close to the angle $\alpha=-\theta$. To reproduce this observation, we assume a piecewise affine variation of f from f_M to a minimal value f_m in the ranges $-\theta\leqslant\alpha\leqslant\beta$, and $\beta-\pi\leqslant\alpha\leqslant-\theta$. The analysis of several images of the bubbles along the obstacle yields the following estimates: $f_m=3.3$ mm and $f_M=4.9$ mm. Given the aspect ratio $a/b=1.6$, we can calculate the drag, lift, and torque from Eq. (2) (Fig. 4).

For the drag, it turns out that the result from Eq. (2) is indiscernible (with 1% precision, up to a free prefactor) with Eq. (1); the agreement with the experimental data is thus quite good [Fig. 4(a)]. For the lift, we predict the sign, i.e., explains the downwards lift: the tensile stress is larger at the trailing edge where it contributes in average downwards (and downstream) for angles between 0° and 90°, than at the leading edge, where it contributes upwards (and upstream). This confirms that the lift is dominated by the elasticity, as is the case for an airfoil [18]. Moreover, we predict correctly the angular dependence of the lift, and a maximum at angle 40°, which agrees quantitatively with the experiments. For the torque, the agreement is qualitative: we predict its sign, the existence of a maximum at an angle smaller than 45°, and the stability (instability) of the parallel (perpendicular) orientations.

The present model relies mainly on the coupling between bubble deformation and flow. This argument has a very general validity: it explains the anti-inertial lift exerted by a flowing foam on an airfoil [18], and predicts quantitatively the drag on a circle on several decades of fluid fractions [12]. It also applies in 3D, as shown by the analogies between the 2D flow around a circle [6] and the 3D flow around a sphere [8,10]. It is qualitatively insensitive to the presence of channel walls, both because this does not influence the convergence or divergence of flow close to the obstacle, and because of the very limited lateral extent of the influence of an obstacle for foams [6,8] compared to Newtonian fluids.

Foams are often modeled as viscoplastic fluids, such as Bingham or Herschel-Bulkley models [24]. Such models describe yielding, which is occurring at the leading side, where the roughly constant amplitude of bubble deformation (Fig. 1) is a manifestation of yield strain. On the other hand, viscoelastic fluids such as the Oldroyd-B model often used for polymers [25] describe the delayed, elastic response of the bubbles, apparent at the trailing side through the progressive stretching of the bubbles (Fig. 1).

Our phenomenological model captures both the coupling between strain and flow (with delayed response) and the saturation of deformation (yielding). It yields a good agreement with experimental data (Fig. 4). Still, we can suggest improvements in three directions. First, the law assumed for f is a phenomenological description of observations. The next step would consist in predicting this function. This would require one to quantify accurately the evolution of

strain due to advection and plastic rearrangements of bubbles, which is predicted by recent models in the simple case of shear flow [5]; here, a generalization to more complex flows and geometries is required. Second, we could extend this model to describe the velocity-dependent contribution to drag, lift, and torque. This requires to quantify precisely the influence of friction on the interaction between bubbles and obstacle boundaries [3]. Third, it would be useful to include the effect of sharp angles, in order to understand why the drag on a square does not depend on its orientation.

We have benefited from stimulating discussions with J. Wang, S. Cox, and C. Raufaste, as well as during the FRIT workshop.

[1] D. Weaire and S. Hutzler, *The Physics of Foams* (Oxford University Press, Oxford, 1999).
[2] R. Höhler and S. Cohen-Addad, J. Phys.: Condens. Matter **17**, R1041 (2005).
[3] N. D. Denkov, V. Subramanian, D. Gurovich, and A. Lips, Colloids Surf., A **263**, 129 (2005).
[4] I. Cantat and R. Delannay, Eur. Phys. J. E **18**, 55 (2005).
[5] D. Weaire, E. Janiaud, and S. Hutzler, e-print cond-mat/0602021.
[6] B. Dollet, F. Elias, C. Quilliet, C. Raufaste, M. Aubouy, and F. Graner, Phys. Rev. E **71**, 031403 (2005).
[7] S. Courty, B. Dollet, F. Elias, P. Heinig, and F. Graner, Europhys. Lett. **64**, 709 (2003).
[8] J. R. de Bruyn, Rheol. Acta **44**, 150 (2004).
[9] M. D. Alonso, S. Hutzler, D. Weaire, and S. J. Cox, in *Proceedings of the 3rd Euroconference on Foams, Emulsions and their Applications*, edited by P. L. J. Zitha, J. Banhard, and P. L. M. M. Verbist (MIT Verlag, Bremen, 2000), p. 282.
[10] I. Cantat and O. Pitois, J. Phys.: Condens. Matter **17**, S3455 (2005).
[11] S. J. Cox, M. F. Vaz, and D. Weaire, Eur. Phys. J. E **11**, 29 (2003).
[12] C. Raufaste, B. Dollet, S. Cox, Y. Jiang, and F. Graner (unpublished).
[13] J. Feng, H. H. Hu, and D. D. Joseph, J. Fluid Mech. **261**, 95 (1994).
[14] J. Happel and H. Brenner, *Low Reynolds Number Hydrodynamics* (Martinus Nijhoff, Den Haag, 1983).
[15] P. Y. Huang, H. H. Hu, and D. D. Joseph, J. Fluid Mech. **362**, 297 (1998).
[16] S. Daugan, L. Talini, B. Herzhaft, and C. Allain, Eur. Phys. J. E **7**, 73 (2002).
[17] Y. J. Liu and D. D. Joseph, J. Fluid Mech. **255**, 565 (1993).
[18] B. Dollet, M. Aubouy, and F. Graner, Phys. Rev. Lett. **95**, 168303 (2005).
[19] E. Janiaud and F. Graner, J. Fluid Mech. **532**, 243 (2005).
[20] J. Wang and D. D. Joseph, J. Fluid Mech. **511**, 201 (2004).
[21] B. Dollet and F. Graner, J. Fluid Mech. (to be published).
[22] E. Mitsoulis, Chem. Eng. Sci. **59**, 789 (2004).
[23] S. Cox, B. Dollet, and F. Graner, Rheol. Acta **45**, 403 (2006).
[24] J. Lauridsen, M. Twardos, and M. Dennin, Phys. Rev. Lett. **89**, 098303 (2002).
[25] R. G. Larson, *The Structure and Rheology of Complex Fluids* (Oxford University Press, New York, 1999).